J Therm Anal Calorim (2011) 103:827–834
DOI 10.1007/s10973-010-1049-5

Structural characterisation and thermo-physical properties of glasses in the Li_2O–SiO_2–Al_2O_3–K_2O system

Hugo R. Fernandes · Dilshat U. Tulyaganov · Ashutosh Goel · José M. F. Ferreira

Received: 4 August 2010 / Accepted: 9 September 2010 / Published online: 25 September 2010

Abstract This article aims to shed some light on the structure and thermo-physical properties of lithium disilicate glasses in the system Li_2O–SiO_2–Al_2O_3–K_2O. A glass with nominal composition $23Li_2O$–$77SiO_2$ (mol%) (labelled as $L_{23}S_{77}$) and glasses containing Al_2O_3 and K_2O with SiO_2/Li_2O molar ratios (3.13–4.88) were produced by conventional melt-quenching technique in bulk and frit forms. The glass-ceramics (GCs) were obtained from nucleation and crystallisation of monolithic bulk glasses as well as via sintering and crystallisation of glass powder compacts. The structure of glasses as investigated by magic angle spinning-nuclear magnetic resonance (MAS-NMR) depict the role of Al_2O_3 as glass network former with four-fold coordination, i.e., Al(IV) species while silicon exists predominantly as a mixture of Q^3 and Q^4 (Si) structural units. The qualitative as well as quantitative crystalline phase evolution in glasses was followed by differential thermal analysis (DTA), X-ray diffraction (XRD) adjoined with Rietveld-reference intensity ratio (R.I.R.) method, Fourier transform infrared spectroscopy (FTIR) and scanning electron microscopy (SEM). The possible correlation amongst structural features of glasses, phase composition and thermo-physical properties of GCs has been discussed.

Keywords Sintering · Thermo-physical properties · Glass · Glass ceramics · Lithium disilicate

H. R. Fernandes · D. U. Tulyaganov · A. Goel · J. M. F. Ferreira (✉)
Department of Ceramics and Glass Engineering, University of Aveiro, CICECO, 3810-193 Aveiro, Portugal
e-mail: jmf@ua.pt

D. U. Tulyaganov
Turin Polytechnic University in Tashkent, 17, Niyazova Str., Tashkent, Uzbekistan 100174

Introduction

Glass-ceramic (GC) materials are obtained by the controlled nucleation and crystallisation of glasses. The choice of glass composition is crucial to ensure that a high rate of internal, rather than surface, nucleation occurs. An excessively high crystal growth rate is to be avoided since such materials do not develop fine-grained microstructure, necessary for the achievement of high mechanical strength [1, 2]. The binary alkali silicate systems show liquid–liquid phase separation or immiscibility at temperatures below the liquidus temperature of crystallisation. This type of phase separation is often called metastable because crystalline phases are more stable than liquid at the temperature of phase separation [1, 3]. The presence of metastable immiscibility region is the main cause of S-like course of the liquidus curve and binary Li_2O–SiO_2 system is a typical example in this regard which demonstrates S-like course of the liquidus curve in silica-rich region. According to Vogel [3], Li_2O–SiO_2 liquids containing less than 30 mol% Li_2O lead to opalescent or opaque glasses on cooling owing to phase separation. However, mechanical properties and chemical durability of these glasses after devitrification are low.

Study of nucleation and crystallisation processes in parent glasses is essential, enabling to produce final materials of desired properties. In the previous study [4], we observed that glasses with composition in the Li_2O–K_2O–Al_2O_3–SiO_2 system comprising equimolar amount of Al_2O_3 and K_2O were prone to volume nucleation and crystallisation, resulting in formation of fine $Li_2Si_2O_5$ (LD) crystals within the temperature interval of 650–900 °C. Also, it has been demonstrated that Al_2O_3 and K_2O might also improve chemical durability of Li_2O–SiO_2 glasses [3, 5, 6].

The aim of this study is to present an in-depth analysis pertaining to study the structure of Li_2O–Al_2O_3–K_2O–SiO_2 glasses and their devitrification mechanism in relevance with Al_2O_3 and K_2O content. Although the role of Al_2O_3 as glass network former with four-fold coordination of Al(IV) species was hypothesised in our previous study [4], we felt the need of investigating this issue in detail so as to gain a better understanding regarding the structural role of Al_2O_3 in these glasses. Therefore, in this study, ^{29}Si and ^{27}Al magic angle spinning-nuclear magnetic resonance (MAS-NMR) have been employed to study glass structure and derive relevant information with respect to the local environment of silicon and aluminium in experimental glasses. The sintering behaviour and properties of the corresponding glass powder compacts have also been targeted in the framework of this investigation, in particular using Fourier transform infrared spectroscopy (FTIR), scanning electron microscopy (SEM), and X-ray diffraction (XRD) to evaluate qualitative and quantitative phase assemblage. The obtained results demonstrated significant differences between binary 23 mol% Li_2O and 77 mol% SiO_2 composition and its Al_2O_3 and K_2O containing derivatives in terms of structure, crystallisation kinetics and thermo-physical properties.

Experimental procedure

Glass preparation

Powders of technical grade SiO_2 (purity > 99.5%) and of reactive grade Al_2O_3 (Alcoa, Germany, purity > 99.5%), Li_2CO_3 and K_2CO_3 (Sigma–Aldrich, Germany, purity > 99.5%) were used to prepare the experimental glasses. Glasses were prepared in both bulk and frit form by melt-quenching technique in Pt crucible. Table 1 presents the composition of the glasses investigated in this study. The addition of Al_2O_3 and K_2O to the binary Li_2O–SiO_2 system was performed on equimolar basis, and the amount of additives decreased from glass G1 to G3. A binary composition $L_{23}S_{77}$, containing the same amount of Li_2O as glass G3, but richer in SiO_2 was also synthesised.

Table 1 Compositions of the experimental glasses

Oxides/mol%	G1	G2	G3	$L_{23}S_{77}$
Li_2O	15.23	19.08	22.96	22.96
K_2O	5.24	3.94	2.63	–
Al_2O_3	5.24	3.94	2.63	–
SiO_2	74.30	73.04	71.78	77.04
$K_2O + Al_2O_3$	10.48	7.88	5.26	0.00

Two sets of bulk glasses for each composition were obtained by pouring the glass melt on preheated bronze mould: (1) the first set of glasses was allowed to cool down in the air; (2) the second set of glasses was subjected to annealing at 450 °C for 1 h. In order to study the evolution of crystalline phases in monolithic glasses, the annealed glasses were cut into cubes ($1 \times 1 \times 1$ cm^3) and heat treated non-isothermally at 550, 650, 750, 800 and 900 °C for 1 h, at heating rate of 2 K min^{-1}.

Glasses in frit form were dried and then milled in a high-speed porcelain mill to obtain fine glass powders with mean particle size of 5–10 μm. Rectangular bars with dimensions of $4 \times 5 \times 50$ mm^3 were prepared by uniaxial pressing (80 MPa). The bars were sintered under non-isothermal conditions for 1 h at 800, 850 and 900 °C using a low heating rate of 2 K min^{-1} aimed to prevent deformation of samples.

Thermo-physical properties of glasses

The glass transition temperature (T_g), softening point (T_s) and coefficient of thermal expansion (CTE) were obtained from dilatometry measurements which were carried out on prismatic glass samples with a cross section of 4×5 mm^2 (Bahr Thermo Analyze DIL 801 L, Hüllhorst, Germany; heating rate 5 K min^{-1}). differential thermal analysis (DTA) of glass grains with sizes in the range of 415–1,000 μm, collected by sieving of grounded non-annealed glass blocks, was carried out in air (Netzsch 402 EP, Germany) from room temperature to 1,000 °C at different heating rates ($\beta = 2$, 5, 10 and 15 K min^{-1}).

Structural characterisation

The ^{29}Si MAS-NMR spectra were recorded on a Bruker ASX 400 spectrometer operating at 79.52 MHz (9.4 T) using a 7-mm probe at a spinning rate of 5 kHz. The pulse length was 2 μs, and a 60-s delay time was used. Kaolinite was used as the chemical shift reference. ^{27}Al MAS-NMR spectra were recorded on a Bruker ASX 400 spectrometer operating at 104.28 MHz (9.4 T) using a 4-mm probe at a spinning rate of 15 kHz. The pulse length was 0.6 μs, and a 4-s delay time was used. $Al(NO_3)_3$ was used as the chemical shift reference.

Sintering and crystallisation behaviour of glass powder compacts

Infrared spectra of the GCs were obtained using an Infrared Fourier spectrometer (FTIR, model Mattson Galaxy S-7000, USA). For this purpose, samples were crushed to powder form, mixed with KBr in the proportion of 1/150 (by weight) and pressed into a pellet using a hand press.

The qualitative and quantitative crystalline phase analysis in the GCs (crushed to particle size < 45 μm) was made by XRD analysis using a conventional Bragg–Brentano diffractometer (Philips PW 3710, Eindhoven, The Netherlands) with Ni-filtered Cu-Kα radiation. The quantitative phase analysis of GCs was made by combined Rietveld-reference intensity ratio (R.I.R.) method. A 10 wt% of corundum (NIST SRM 676a) was added to all the GC samples as an internal standard. The mixtures, ground in an agate mortar, were side loaded in aluminium flat holder to minimise the problems to due to non-random orientations. Data were recorded in 2θ range $= 5$–115° (step size 0.02°/50 s). The phase fractions extracted by Rietveld refinements, using GSAS-EXPGUI software [7] were rescaled on the basis of the absolute weight of corundum originally added to their mixtures as an internal standard, and therefore, internally renormalised. The background was successfully fitted with a Chebyshev function with a variable number of coefficients depending on its complexity. The peak profiles were modelled using a pseudo-Voigt function with one Gaussian and one Lorentzian coefficient. Lattice constants, phase fractions, and coefficients corresponding to sample displacement and asymmetry were also refined.

Microstructural observations were done on polished (mirror finishing) surface of samples (etched by immersion in 2 vol% HF solution for 2 min) by scanning electron microscopy (SEM; SU-70, Hitachi, Japan).

Results and discussion

Bulk glasses

Glass casting ability

Transparent and colourless glasses G1, G2 and G3 were obtained by melting at 1,550 °C for 1 h, while in case of $L_{23}S_{77}$ transparent melt transformed into a cloudy hazy glass on cooling. Figure 1 shows both the appearance of the experimental non-annealed glasses and the corresponding microstructures which reveal the precipitation of a nanosize droplet phase in glassy matrices suggesting the occurrence of liquid–liquid phase separation in all the 'investigated compositions. However, the phase separation phenomenon was not observed at naked eye for compositions G1, G2 and G3 comprising Al_2O_3 and K_2O. The mean droplet diameter and the population density of droplets (Fig. 1) diminished by increasing amount of Al_2O_3 and K_2O in the Li_2O–SiO_2 system. Consequently, G1 possesses a microstructure comprising rarer smaller droplets compared to the other compositions, evidencing that Al_2O_3 has a strong tendency to reduce phase separation.

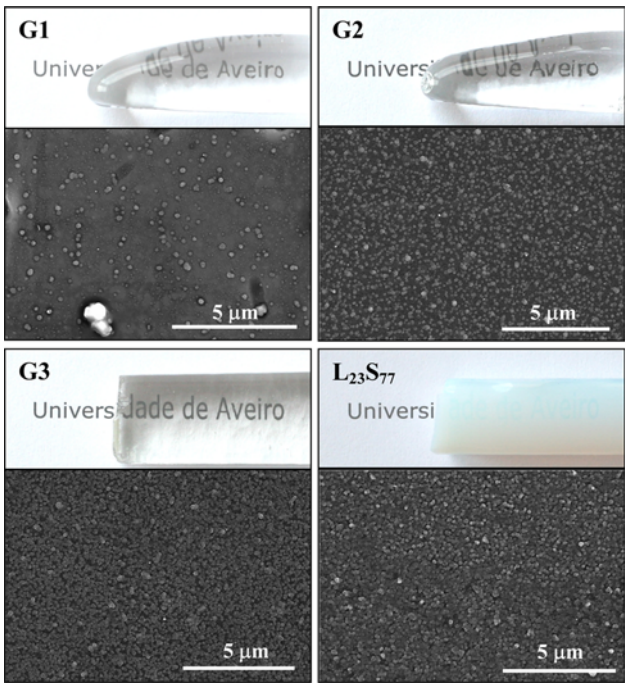

Fig. 1 Physical appearance of the experimental nonannealed bulk glasses and their respective SEM images for glass compositions G1, G2, G3 and $L_{23}S_{77}$, respectively

The finer scale morphology and a relatively lower volume fraction of the droplets observed in the glasses G1, G2 and G3 result in the nonexistence of Tyndall effect which can explain the homogeneous and transparent appearance in this compositions when observed with naked eye [3]. On the other hand, the bigger droplets and their higher concentration presented in the microstructure of composition $L_{23}S_{77}$ lead to the cloudy appearance, as expected since the droplet size in this glass has remained nearly the same as observed by Vogel in Li_2O–SiO_2 glasses [3].

Thermo-physical properties and structural features of the glasses

The addition of Al_2O_3 and K_2O in the as-investigated proportions favoured an increase in T_g and T_s of the glasses (Fig. 2a, b). From the linear part of the dilatometric curves, the values of $CTE_{200–400\ °C}$ for glasses G1, G2, G3 and $L_{23}S_{77}$, were obtained as 8.47, 8.69, 9.65 and $8.16 \times 10^{-6}\ K^{-1}$, respectively. Considering that Al^{3+} acts as a network former, the number of non-bridging oxygens per each tetrahedral cation (NBO/T) suggested more polymerised glass network structures for G1 (NBO/T = 0.36) and G2 (NBO/T = 0.47) than for G3 (NBO/T = 0.60) and $L_{23}S_{77}$ (NBO/T = 0.60). Diminishing the NBO/T led to an increase in T_g and decrease in CTE values. The higher CTE value of glass G3 compared with $L_{23}S_{77}$ can be explained by the effect of incorporation of

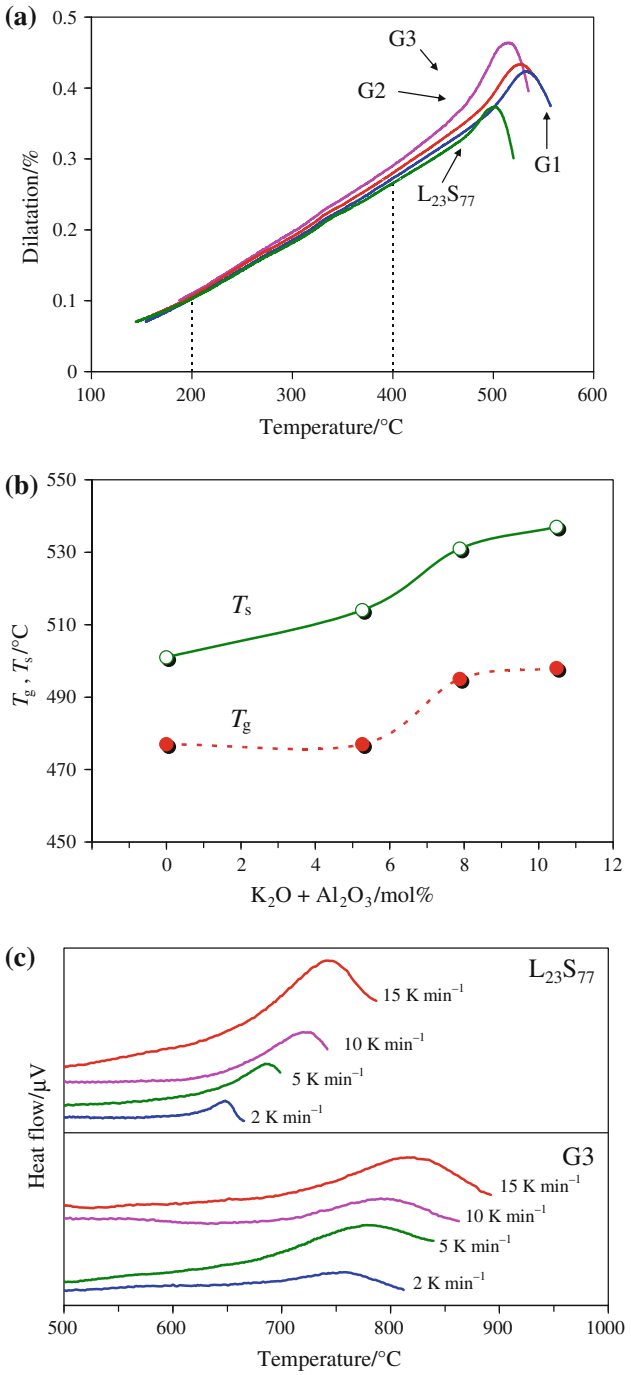

Fig. 2 Thermo-physical properties of the experimental annealed bulk glasses (K_2O and Al_2O_3 content in mol%): **a** Dilatometry, **b** T_g and T_s versus additives content, and **c** differential thermal analysis (DTA) thermograph of glasses G3 and $L_{23}S_{77}$ at different heating rates ($\beta = 2, 5, 10$ and 15 K min^{-1})

potassium cation in the glass network. In general, alkali ions fill up the glass structure interstices, thus preventing bond bending which consequently increases CTE. This effect, however, can be compensated by addition of intermediate oxides (such as Al_2O_3) that reduce the concentration of NBOs, provided that molar concentration of Al does not exceed that of the charge-balancing cations (e.g. alkalis) [1].

Figure 2c presents the DTA thermographs of glasses G3 and $L_{23}S_{77}$ at different heating rates to reveal the influence of $Al_2O_3 + K_2O$ introduction on devitrification behaviour of glass $L_{23}S_{77}$. As is evident from Fig. 2c, the crystallisation curve for glass G3 is shallower and exhibits a considerable shift to high temperature with respect to glass $L_{23}S_{77}$. These data clearly demonstrate stronger ability of glass $L_{23}S_{77}$ for devitrification due to coarser scale morphology and a relatively higher volume fraction of the droplets observed in parent glass (Fig. 1d). Similar to the other glasses in the Li_2O–SiO_2 system containing less than 30 mol% Li_2O, nucleation in $L_{23}S_{77}$ glasses was initiated by metastable liquid–liquid immiscibility [3] that was more extended than in Al_2O_3 and K_2O containing derivates. The activation energy of crystallisation (E_c) as obtained in our previous study for glasses $L_{23}S_{77}$ and G3 are 153 and 330 kJ mol^{-1} [4], respectively, reflecting the structural role of Al_2O_3 which is probably contributing towards decreasing the immiscibility trend, thus reducing mobility of the glass-forming ions and ionic complexes operative in the crystallisation process.

The ^{29}Si and ^{27}Al MAS-NMR spectra of the samples (Fig. 3a, b, respectively) exhibit broad bands which indicate the amorphous nature of investigated materials [8, 9]. Glass $L_{23}S_{77}$ exhibited two characteristic peaks in ^{29}Si MAS-NMR spectra at about −92 and −108 ppm (Fig. 3a), which can be assigned to a mixture of Q^3 and Q^4 species, respectively. The addition of Al_2O_3 and K_2O resulted in a broadening of spectra and shifting the peak centred at −92 ppm to lower values. These features imply towards decreasing number of Q^3 species at the expense of more polymerised Q^4 units and are consistent with calculated NBO/T, evolution of CTE, T_g and T_s values.

The ^{27}Al MAS-NMR data are shown in Fig. 3b. A signal at ~52 ppm evidenced about dominant presence of tetrahedral aluminium in all the $Al_2O_3 + K_2O$ containing glasses and especially in G1 and G2. It is noteworthy that Al(IV) species are characteristic networking-forming units of aluminosilicate glasses causing increase in crosslinking of the glass structure [10]. Therefore, as the sum of Al_2O_3 and K_2O increased the ($AlO_{4/2}$) glass forming units are incorporated in the network as Q^4 species. To maintain local charge neutrality, $(AlO_{4/2})^-$ units will be charge compensated by alkali cations (K^+, Li^+) which must be present in the vicinity of each such tetrahedron. The results of ^{27}Al MAS-NMR study strongly support our previous presumption [4] concerning the role of Al_2O_3 as glass network former with four-fold coordination of Al(IV) species in the experimental compositions G1, G2 and G3 [10, 11].

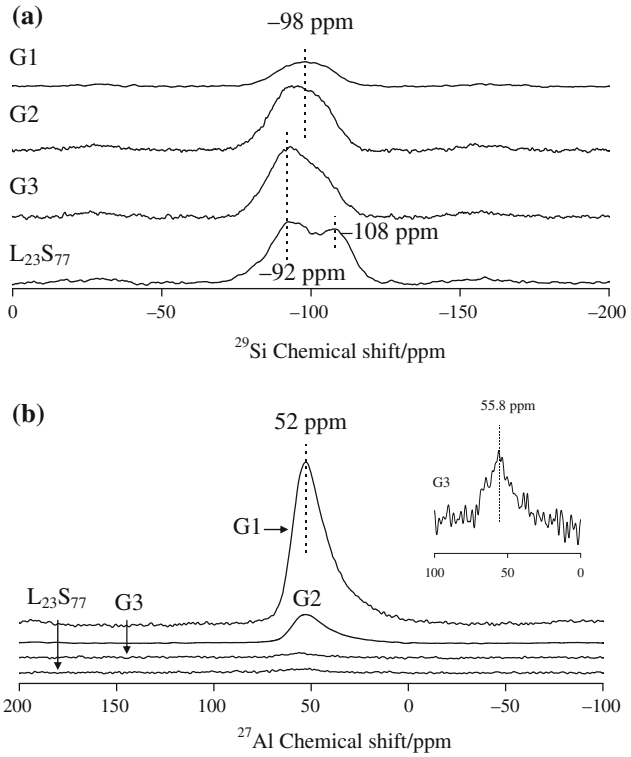

Fig. 3 ^{29}Si MAS-NMR (**a**) and ^{27}Al MAS-NMR (**b**) spectra of glasses. The insertion shows the ^{27}Al MAS-NMR spectrum for glass G3

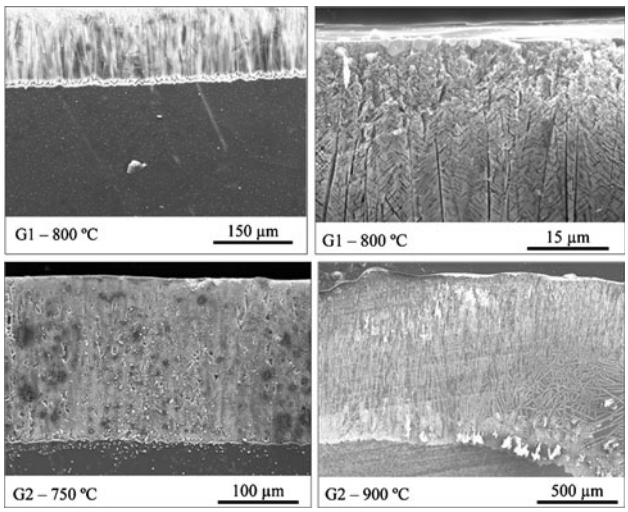

Fig. 4 SEM of bulk glasses heat treated at different temperatures

Surface crystallisation and dendritic skeletal crystal growth which can be observed in SEM images of both G1 and G2 glasses (Fig. 4), being a further evidence of the structural role of Al^{3+} that apparently increased viscosity of those glasses and greatly decreased the immiscibility trends. On the contrary, fine grained volume crystallisation has been observed in low alumina G3 glass [4].

Glass powder compacts

Well-sintered GCs demonstrating flexural strength values 114 ± 2, 158 ± 5 and 81 ± 8 MPa for G1, G2 and G3, respectively, were obtained after heat treatment of glass powder compacts at 800 °C for 1 h. Further heat treatment at 850 °C significantly improved densification of G3 compared to G1 and G2 whereas maximum bending strength values as 189 ± 8 (G1), 195 ± 9 (G2) and 224 ± 4 (G3) MPa were revealed after sintering at 900 °C for 1 h. Figure 5 presents the SEM images of glass powder compacts G1 and G3 heat treated at 800, 850 and 900 °C. At the lowest temperature, structural features of Li_2SiO_3 (LS) crystals which possess a chain silicate structure and crystallised dendritically can be observed. It is known that LS crystals are particularly easy to dissolve from GC by dilute hydrofluoric acid while the surrounding aluminosilicate glassy matrix is considerably more resistant to acid attack [2]. At 850 °C, LD crystals start up to grow in the form of submicron-sized rods and act as nucleating sites for new rods. LD crystals uniformly embedded in glassy matrix were responsible for high mechanical strength of these GCs at 900 °C. According to XRD data (spectra are not shown), LS was revealed as the single crystalline phase in GC1 after sintering at 800 °C, while GC2 and GC3 comprised LS along with quartz (Q) and LD as minor phases. At 850 and 900 °C, GC3 exhibited almost monomineral composition of LD with peaks of low intensity attributed to quartz. In compositions G1 and G2, both LS and Q were found as minor crystalline phases at 850 and 900 °C. Unlike Al_2O_3 and K_2O containing GCs, binary $L_{23}S_{77}$ composition featured very poor sinterability thus exhibiting bending strength of 13 ± 2 MPa and density of 2.14 ± 0.04 g cm^{-3} at 900 °C for 1 h (Fig. 5a). This phenomenon can be explained by lower E_c for $L_{23}S_{77}$ compared to G3 causing formation of large fraction of LD phase that hinders the densification process [12]. Indeed, LD was the main crystalline phase in $L_{23}S_{77}$ glass powder compacts sintered at 800 and 850 °C. At 900 °C both LD along with quartz became the principal crystalline phases while tridymite along with cristobalite were also recorded.

The FTIR spectra of glass powder compacts heat treated at 800, 850 and 900 °C are presented in Fig. 6. In all Al_2O_3 and K_2O containing compositions. transmittance bands of LS phase, i.e. 525–527, 604, 635–638, 728–732, 846–851, 932, 973 and 1,054–1,057 cm^{-1} were revealed at lower temperatures [13]. For instance, FTIR spectrum of G1 at 800 °C exhibited well resolved bands at ~527, 609, 730, 850 and 923 cm^{-1}, and a shallow band at ~1,060 cm^{-1}, which resembles the above mentioned typical values for LS (Fig. 6a). The absence of other significant bands suggested that LS is the only crystalline phase formed in G1 at this temperature. The sharpness and intensity of these bands

tend to be diminished and shifted slightly to higher frequency values with increasing sintering temperature. Thus, at 850 °C new peaks characteristic for transmittance of LD phase were revealed and become more pronounced at 900 °C. The FTIR patterns of G2 and G3 glasses sintered at 800 °C (Fig. 6b) are quite similar to spectrum of G1. However, transmittance bands in the spectra of G1, G2 and G3 at 850 and 900 °C mostly correspond to LD crystalline phase. Binary Al_2O_3 and K_2O free $L_{23}S_{77}$ composition featured several peaks at ~475, 563, 633, 760, 788, 940 and 1,108 cm^{-1} (Fig. 6d). These transmittance bands can be assigned to LD control-crystal (470, 548, 635, 756, 782, 936, 1,022, 1,108 and 1,212 cm^{-1}) [13]. At 850 and 900 °C FTIR spectra presented similar profile coupled with appearance of small peaks at ~450 and 692 cm^{-1} corresponding to standard quartz [14].

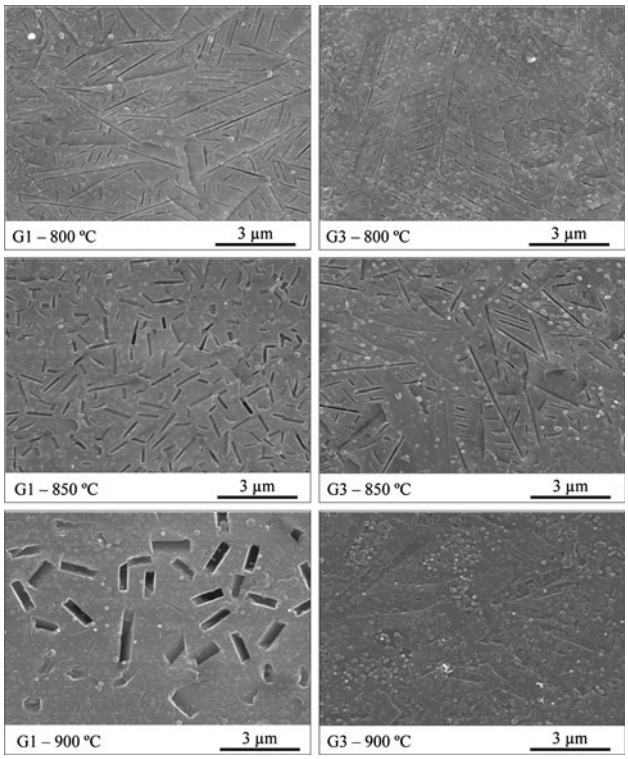

Fig. 5 SEM of glass powder compacts G1 and G3 heat treated at 800, 850 and 900 °C

From the hot stage microscopy observation performed in the previous study two main steps of sintering were revealed for G1, G2 and G3 compositions [4]. First sintering step was initiated at temperatures slightly higher than T_g and retarded by crystallisation of LS at around 600 °C whereas a second shrinkage step started almost synchronically at about 800 °C for all Al_2O_3 and K_2O containing compositions. Moreover, the interval for first sintering step was wider for G1 (68 °C) and G2 (49 °C) than for G3 (45 °C).

Nevertheless, deeper investigation was required for quantifying content of crystalline and amorphous phase. Therefore, Rietveld-R.I.R. refinement was conducted for the samples sintered at 800 and 850 °C, i.e. in the interval when a second phase of sintering took place and was accompanied with new phase transformations. From Fig. 7a, it is clear that $L_{23}S_{77}$ composition at 800 °C contained about 53.0 wt% LD, 3.4 wt% quartz and 43.6 wt% amorphous phase. In comparison to $L_{23}S_{77}$, compositions G1, G2 and G3 featured lower crystalline content (mainly LS and quartz), but higher amount of residual amorphous

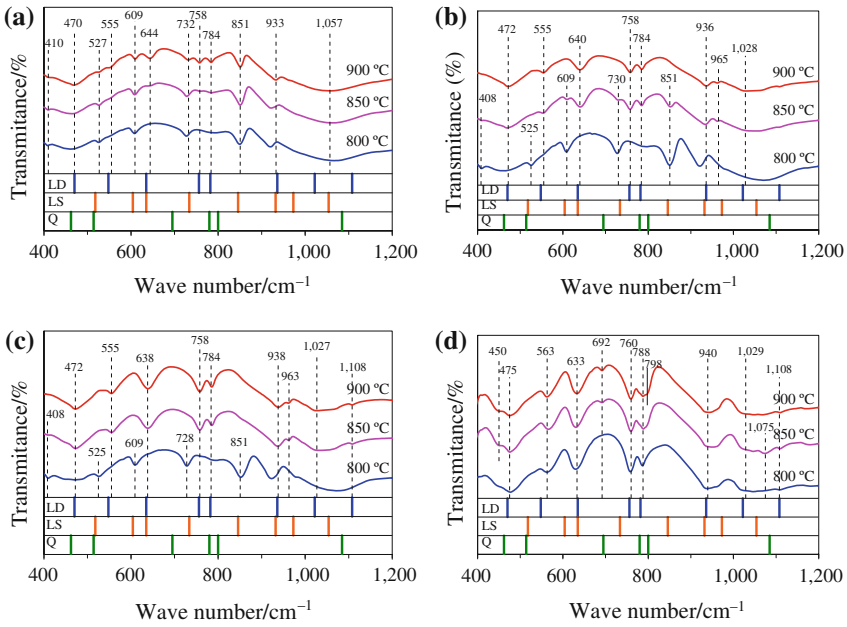

Fig. 6 FTIR spectra of the investigated glass powder compacts (a) G1, (b) G2, (c) G3 and (d) $L_{23}S_{77}$ after heat treatment at 800, 850 and 900 °C for 1 h, respectively. Typical spectra for quartz (Q), lithium disilicate (LD) and lithium metasilicate (LS) are indicated in the figure

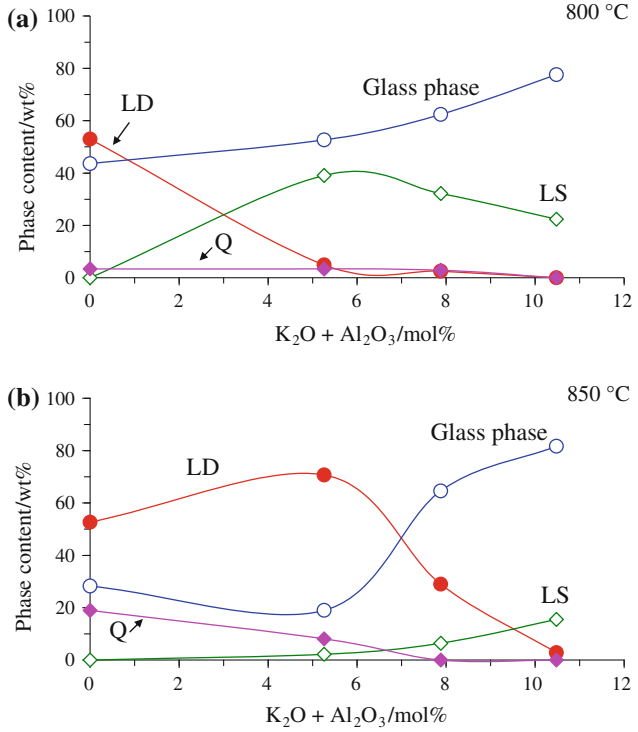

Fig. 7 Quantitative crystalline phase evolution in GCs as obtained from Rietveld-R.I.R. refinement at **a** 800 °C and **b** 850 °C. Phases are indicated in the figure as Q (quartz, SiO_2), LD (lithium disilicate, $Li_2Si_2O_5$) and LS (lithium metasilicate, Li_2SiO_3)

reservoir (52.7, 62.4 and 77.6 wt% for G3, G2 and G1, respectively). After heat treatment at 850 °C, no deviation in LD content was revealed in $L_{23}S_{77}$ although quartz content increased up to 19 wt% at the expense of silica rich amorphous phase (Fig. 7b). It is due to the precipitation of residual silica glassy phase (density 2.20 g cm^{-3}) in the form of quartz (density 2.65 g cm^{-3}) that overall volume of the system decreased. However, the occurred volume changes were not sufficient to cause appreciable increase of density and mechanical strength even after 900 °C.

Unlike $L_{23}S_{77}$, the volume changes in G3 at 850 °C were associated with both reaction of residual glass with LS causing formation of large fraction LD (up to 70.7 wt%) and simultaneous densification of residual amorphous phase owing to its lower crystallinity (Fig. 7a). The densification was less pronounced in G2 and G1 since LD was formed in low amount and mostly due to reaction between LS and quartz whereas the amount of glassy phase remained almost constant. The reason for this was that significant level of densification of G1 and G2 was attained during the first sintering stage before crystallisation started [4]. Formation of LD was advanced in G2 and mostly in G1 in the interval 850–900 °C. The results of Rietveld-R.I.R. refinement are well correlated with the viscosity–temperature curves for G1, G2 and G3 glasses [4] evidencing that the glass G3 exhibited lowest viscosity at temperatures below 850 °C and at the constant temperature $\log \eta_{(G1)} > \log \eta_{(G2)} > \log \eta_{(G3)}$. The opposite trend was observed at temperatures higher than 850 °C when compositions G2 and G3 demonstrated higher viscosity than G1. This can be explained by formation of a larger fraction of LD in GC3 and GC2 at 850 °C (Fig. 7b).

Conclusions

This study demonstrates that slight changes in lithium silicate glass composition may have significant effects on chronology and morphology of phases. A careful selection of additive's amount is crucial to ensure that internal nucleation and moderate crystal growth rate in parent glass occurs. The following conclusions can be drawn from the above discussed results:

1. Liquid–liquid phase separation occurred in all the investigated monolithic bulk glasses. The mean droplet diameter and the population density of droplets diminished by increasing amount of Al_2O_3 and K_2O demonstrating that aluminium greatly decreased the immiscibility trends in the Li_2O–SiO_2 system.
2. Al_2O_3- and K_2O-free $L_{23}S_{77}$ glass demonstrated higher rate of crystal growth due to extended phase separation.
3. The addition of Al_2O_3 and K_2O in the as-investigated proportions favoured the decrease of CTE and an increase of T_g and T_s. The surface crystallisation and dendritic skeletal crystal growth was observed in compositions G1 and G2 with higher Al_2O_3 and K_2O content whereas bulk crystallisation with fine-grained microstructure has been attained in low alumina G3 glass.
4. ^{29}Si MAS-NMR spectra evidenced a decreasing number of Q^3 species at the expense of Q^4 implying towards polymerised structure of Al_2O_3 and K_2O containing compositions.
5. The peaks of ^{27}Al MAS-NMR spectra of G1 and G2 glasses were centred at ~52 ppm corresponding to tetrahedral four-coordinated Al(IV) species confirming the role of Al_2O_3 as glass network former.
6. The sintering and crystallisation of Al_2O_3- and K_2O-containing compositions in the silica reach region of Li_2O–SiO_2 system, which resulted in well-densified and mechanically strong fine-grained GCs with LD as the major crystalline phase.
7. Glass G3 exhibited most promising thermo-physical properties due to careful selection of Al_2O_3 and K_2O additives promoting internal nucleation and moderate crystal growth rate.

Further investigations of new materials will be required to study chemical durability, mechanical properties

(fracture toughness, Weibull modulus, etc.) as well as to optimise their processing parameters.

Acknowledgements Hugo R. Fernandes is grateful for the financial support of CICECO and for the PhD grant (SFRH/BD/41307/2007) from the FCT, Portugal. Ashutosh Goel is thankful to CICECO and FCT, Portugal (SFRH/BPD/65901/2009) for the post-doctoral research grant.

References

1. Shelby JE. Introduction to glass science and technology. Cambridge: The Royal Society of Chemistry; 2005.
2. Höland W, Beall G. Glass-ceramic technology. Ohio: The American Ceramic Society; 2002.
3. Vogel W. Structure and crystallization of glasses. 1st ed. Oxford: Pergamon Press; 1971.
4. Fernandes HR, Tulyaganov DU, Goel A, Ribeiro MJ, Pascual MJ, Ferreira JMF. Effect of Al_2O_3 and K_2O content on structure, properties and devitrification of glasses in the Li_2O–SiO_2 system. J Eur Ceram Soc. 2010;30:2017–30.
5. Barrett JM, Clark DE, Hench LL. Glass–ceramic dental restoration. U.S. Patent. 1980;4:189–325.
6. Wu M, Cannon WR, Panzera C. Castable glass–ceramic composition useful as dental restorative. U.S. Patent. 1985;4:515–634.
7. Larson AC, von Dreele RB. GSAS: general structure analysis system LANSCE, MS-H805. Los Alamos: Los Alamos National Laboratory; 1998.
8. Engelhardt G, Nofz M, Forkel K, Wihsmann FG, Magi M, Samoson A, Lippmaa E. Structural studies of calcium aluminosilicate glasses by high resolution solid state ^{29}Si and ^{27}A1 magic angle spinning nuclear magnetic resonance. Phys Chem Glasses. 1985;26:157–65.
9. Mackenzie KJD, Smith ME. Multinuclear solid-state NMR of inorganic materials. Amsterdam: Pergamon; 2002.
10. Abo-Mosallam HA, Hill RG, Karpukhina N, Law RV. MAS-NMR studies of glasses and glass-ceramics based on a clinopyroxene–fluorapatite system. J Mater Chem. 2010;20:790–7.
11. Stebbins JF, Kroeker S, Lee SK, Kiczenski TJ. Quantification of five- and six-coordinated aluminium ions in aluminosilicate and fluoride-containing glasses by high-field, high-resolution ^{27}Al NMR. J Non-Cryst Solids. 2000;275:1–6.
12. Silgardi C, D'Arrigo MC, Leonelli C. Sintering behaviour of glass ceramics frits. Am Ceram Soc Bull. 2000;9:88–93.
13. Fuss T, Mogus-Milankovic A, Ray CS, Lesher CE, Youngman R, Day DE. Ex situ XRD, TEM, IR, Raman and NMR spectroscopy of crystallization of lithium disilicate glass at high pressure. J Non-Cryst Solids. 2006;352:4101–11.
14. Bhaskar JS, Parthasarathy G, Sarmah NC. Fourier transform infrared spectroscopic estimation of crystallinity in SiO_2 based rocks. Bull Mater Sci. 2008;31(5):775–9.